Vibrational Spectroscopy xxx (2016) xxx–xxx

Contents lists available at ScienceDirect

Vibrational Spectroscopy

journal homepage: www.elsevier.com/locate/vibspec

Ultrafast broadband Fourier-transform CARS spectroscopy at 50,000 spectra/s enabled by a scanning Fourier-domain delay line

Miu Tamamitsu[a], Yusuke Sakaki[a], Tasuku Nakamura[a], G. Krishna Podagatlapalli[a], Takuro Ideguchi[b,*], Keisuke Goda[a,c,d]

[a] Department of Chemistry, University of Tokyo, 7-3-1 Hongo, Bunkyo-ku, Tokyo 113-0033, Japan
[b] Research Centre for Specrochemistry, University of Tokyo, 7-3-1 Hongo, Bunkyo-ku, Tokyo 113-0033, Japan
[c] Department of Electrical Engineering, University of California, Los Angeles, CA 90095, USA
[d] Japan Science and Technology Agency, 7 Gobancho, Chiyoda-ku, Tokyo 102-0076, Japan

ARTICLE INFO

Article history:
Received 29 April 2016
Received in revised form 11 July 2016
Accepted 11 July 2016
Available online xxx

Keywords:
Raman spectroscopy
Coherent anti-Stokes Raman scattering
Fourier-transform spectroscopy

ABSTRACT

We propose and demonstrate a coherent Raman scattering (CRS) spectroscopy technique capable of acquiring 50,000 broadband Raman spectra/s. This ultrafast spectral acquisition is realized by employing a Fourier-domain delay line based on a rapidly rotating polygonal mirror array as an optical path-length scanner in a broadband Fourier-transform coherent anti-Stokes Raman scattering (FT-CARS) spectroscopy platform. We provide a theoretical description of the proposed FT-CARS spectroscopy technique while also presenting its proof-of-concept demonstration on a liquid toluene sample. Our use of a 54-facet polygonal mirror array rotating at 916 rotations/s achieves a record high scan rate of 50,000 CARS spectra/s, covering most of the molecular fingerprint region (200–1430 cm^{-1}) with a high resolution of 4.2 cm^{-1}. This ultrafast broadband CRS technique is expected to be of great use in applications where high-throughput screening or real-time monitoring of unknown samples with high specificity is required, such as single-cell analysis and biomedical imaging.

1. Introduction

Coherent Raman scattering (CRS) such as stimulated Raman scattering (SRS) and coherent anti-Stokes Raman scattering (CARS) spectroscopy is a useful tool in biochemistry [1–8] and medicine [9–12] as it offers the sample's intrinsic molecular vibrational information in a non-invasive, label-free manner [3,4]. For such use, acquisition of a broadband Raman spectrum is powerful since it enables accurate identification of unknown chemical ingredients [1,3–8,10–12]. At the same time, high-speed Raman spectral acquisition is also critical in applications where high-throughput screening or real-time multi-dimensional monitoring of moving targets [10,12] is required. For these purposes, various CRS spectroscopy techniques have been developed. To acquire broadband (>1000 cm^{-1}) Raman spectra, one approach aims to detect a spatially dispersed spectrum of a CARS [6,13] or SRS [14] beam with a multi-channel detector, achieving up to ~3000 cm^{-1} [6,14]. However, the acquisition rates of the previous demonstrations are limited to ~10,000 spectra/s [14] while being intrinsically limited by the readout speed of their sensitive one-dimensional camera. Another approach based on a frequency-swept laser in SRS spectroscopy [15] is useful for higher-speed CRS imaging applications, achieving 30.8 spectral frames/s with a resolution of 500 × 480 pixels/frame. However, its frequency sweep can only be performed in a frame-by-frame manner, which limits the spectrum acquisition speed, while the accessible Raman spectral bandwidth is limited to 300 cm^{-1}.

One way of breaking this speed-bandwidth trade-off is to simultaneously detect broadband CRS signals at a very high speed and numerically demultiplex them afterwards [16–25]. One of such SRS spectroscopy techniques has been recently reported [24] where each SRS field is tagged by a certain MHz frequency via a MHz spectral intensity modulation of the femtosecond pump laser, which are separated through Fourier transformation after a superimposed waveform of all the SRS fields is rapidly detected by a fast-reading single-pixel photodiode. The technique achieves a high acquisition rate of 17,000 spectra/s although the Raman spectral bandwidth is yet limited to ~200 cm^{-1}. Meanwhile, the CARS counterpart of the approach, called Fourier-transform CARS

* Corresponding author at: Research Centre for Spectrochemistry, University of Tokyo, 7-3-1 Hongo, Bunkyo-ku, Tokyo 113-0033, Japan.
E-mail addresses: ideguchi@chem.s.u-tokyo.ac.jp, t.ideguchi@gmail.com (T. Ideguchi).

http://dx.doi.org/10.1016/j.vibspec.2016.07.007

(FT-CARS) spectroscopy, has been studied for several years [16–23,25]. While we review the principles of FT-CARS spectroscopy in the subsequent section, the latest technique enabled by a resonant-scanner-based optical delay line [25] has been developed to achieve an acquisition rate of 24,000 spectra/s over a Raman spectral region of 200–1500 cm^{-1}, covering most of the molecular fingerprint region with a spectral resolution of 10 cm^{-1}. The use of a more rapidly scanning optical delay line can further enhance the acquisition rate of FT-CARS spectroscopy without sacrificing the spectral bandwidth and resolution.

Here we propose and demonstrate a FT-CARS spectroscopy technique that achieves a record-high spectral acquisition rate of 50,000 spectra/s over a Raman spectral region of 200–1430 cm^{-1} with a spectral resolution of 4.2 cm^{-1}. The enabling component of the technique is a Fourier-domain delay line consisting of a grating-based 4f pulse shaper combined with a rotating polygonal mirror array whose reflecting facets are placed in the Fourier plane [26,27]. The rotating tilted reflection of the spectrum around the Fourier plane introduces a time-varying linear phase ramp to the pulse laser's spectrum which essentially causes an increasing temporal delay to the pulse envelope. The combination of the scanning mirror array's fast mechanical rotation and polygonal shape enables continuous Raman spectral acquisition at a high refreshing rate. In the following sections, we first review the principles of FT-CARS spectroscopy and theoretically analyze its performance when combined with a polygonal Fourier-domain delay line. As a proof-of-concept demonstration, we implement a 54-facet polygonal mirror array rotating at 916 rotations/s (rps) to perform fast continuous broadband Raman spectroscopy and use the system to probe a liquid toluene sample. Our technique is expected to be of great use in applications where high-throughput screening or real-time monitoring of unknown samples with high specificity is required, such as single-cell analysis and biomedical imaging.

2. Theory of FT-CARS spectroscopy with a polygonal Fourier-domain delay line

2.1. Principles of FT-CARS spectroscopy

We start with the principles of FT-CARS spectroscopy which is at the basis of our technique. As shown in Fig. 1(a), a femtosecond pulse laser beam with a pulse repetition rate of f_{rep} is split by a beamsplitter into two arms of a Michelson interferometer. The end mirror in one of the arms (reference arm) is fixed while the end mirror in the other arm (scanning arm) is scanned in time. Assuming that the scanned pulse train's interval between consecutive pulses is $1/f_{rep} + \Delta t$, for every pair of nearby scanned and reference pulses, the CARS process starts with the excitation of the sample by the reference pulse. The use of the femtosecond pulse laser enables coherent excitation of every molecular vibrational mode within the laser's broad spectral bandwidth. The subsequent scanned pulse either amplifies or weakens the coherent molecular vibration (i.e., it loses or gains energy, respectively), depending on its arrival time [28], indicating that the molecule's vibrational signature is encoded onto the time-domain waveform of the resulting blue-shifted anti-Stokes beam as shown in Fig. 1(b). Here, as shown in Fig. 1(c), an optical long-pass filter may be installed before the sample to sharply cut the excitation laser's spectrum, so that the blue-shifted anti-Stokes beam can be effectively extracted by a subsequent short-pass filter. The extracted beam is focused onto the single-pixel photodiode to read out its waveform, which is digitized and finally processed by the computer to retrieve the CARS spectrum.

For quantitative discussion, note that while the molecular vibration is probed with a constant temporal resolution of Δt, since each CARS process is probed with a refreshing period of $1/f_{rep}$, the detected waveform is a replica of the molecular vibration whose frequency is down-converted by a factor of

$$F = f_{rep}\Delta t. \quad (1)$$

This down-conversion factor F maps the THz frequency of the molecular vibration to a detectable MHz frequency, enabling a fast direct readout of the molecular vibration with the single-pixel photodiode. The CARS spectrum of the sample can be retrieved by Fourier-transforming the acquired time-domain signal known as a CARS interferogram that consists of multiple down-converted molecular vibrational frequencies. Here, the non-resonant background, which is a result of instantaneous electronic transitions, can be eliminated by filtering out the zero-temporal-delay region of the interferogram [19]. Meanwhile, the higher-frequency limit f_{high} of the Raman spectral region is given by the bandwidth Δf_{high} of the frequency components that induce the CARS process as

$$f_{high} = \Delta f_{high}, \quad (2)$$

whereas the lower-frequency limit is defined by the frequency difference Δf_{low} between the optical long-pass and short-pass boundary frequencies. However, due to the Nyquist-Shannon sampling theorem, a frequency that can be recovered from the pump-probe measurement is also limited to half of the pulse repetition frequency, limiting the accessible Raman spectral region to be

$$f_{high} = \frac{f_{rep}}{2F}. \quad (3)$$

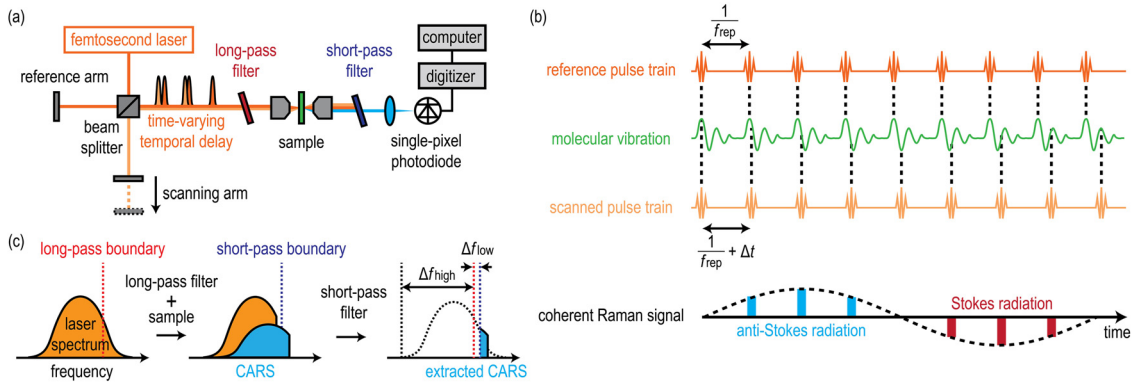

Fig. 1. FT-CARS spectroscopy. (a) Schematic of a basic FT-CARS spectroscopy setup. (b) Temporal representation of the generation of a FT-CARS signal resulting from one molecular vibrational mode. (c) Extraction of anti-Stokes radiation limiting the accessible Raman spectral region.

Please cite this article in press as: M. Tamamitsu, et al., Ultrafast broadband Fourier-transform CARS spectroscopy at 50,000 spectra/s enabled by a scanning Fourier-domain delay line, Vib. Spectrosc. (2016), http://dx.doi.org/10.1016/j.vibspec.2016.07.007

Eqs. (2) and (3) indicate that $\Delta f_{\text{high}} \leq f_{\text{rep}}/2F$ should be satisfied for ideal performance.

2.2. Principles of a polygonal Fourier-domain delay line

Our technique is FT-CARS spectroscopy with the scanner in the scanning arm replaced by a polygonal Fourier-domain delay line. As shown in Fig. 2(a), it consists of a grating-based reflective 4f pulse shaper with a rotating facet of a polygonal scanning mirror array placed in its Fourier plane. The dispersed spectrum of the pulse laser beam is focused onto the Fourier plane so that the tilted mirror facet reflects the spectrum at the angle of θ from its normal reflection. This rotating tilted reflection produces a time-increasing linear phase ramp to the spectrum of the pulse which, from the Fourier-transform theory, corresponds to a time-increasing temporal shift of its envelope. After the spectrum is recombined through the same lens and grating, the beam exits the grating along a shifted optical path parallel to the incident beam. By slightly shifting the lens upwards, the beam exits at a higher position than the incident beam as shown by the side view in Fig. 2(a), enabling us to utilize both the negative and positive reflecting angles of θ. A mirror reflects this beam perpendicularly and restores it to the identical optical path as it has travelled. The beam finally exits the delay line following the same optical path as the incident beam in the opposite direction. Note that since the scanning mechanism is based on the rotational motion, its speed is less restricted by inertia than is the resonant-scanner employed in Ref. [25], which allows us to achieve a much higher scanning rate when using a large number of polygonal mirror facets.

2.3. Group delay and duty cycle

To predict the performance of our FT-CARS spectroscopy technique, we first theoretically analyze the polygonal Fourier-domain delay line in terms of (1) the group delay of an output pulse and (2) the duty cycle. The group delay can be quantified by analyzing the phase change gained by each spectral component through the pulse shaper. The analysis given in Ref. [27] indicates that its effective phase increase results from a geometrical path-length difference produced by the tilted reflection around the Fourier plane. Here, we trace the ray of a spectral component which is shifted by a distance of h apart from the axis of the 4f pulse shaper. As indicated by points A and B in Fig. 2(b), the tilting angle of θ shortens the path length by $2\Delta l$ which can be found to be [26]

$$\begin{aligned} 2\Delta l &= 2\left[h - x_0 + R\tan\left(\frac{\theta}{2}\right)\right]\tan\theta \\ &= 2h\tan\theta - 2[R(1-\sec\theta) + x_0\tan\theta], \end{aligned} \tag{4}$$

where R is the inner radius of the polygonal mirror array and x_0 is the offset distance of the mirror array's center from the axis of the 4f pulse shaper. From the first-order grating equation, an approximation $h \approx l_f(N\lambda - \sin\alpha)$ can be used, where l_f is the focal length of the lens, N is the grating frequency, λ is the wavelength of the spectral component, and α is the incident angle of the beam to the grating. Since the path-length difference is doubled by the restoring mirror, the effective phase increase p with respect to $\theta = 0$ is given by

$$\begin{aligned} p(\theta,\omega) &= -\frac{4[\Delta l(\theta) - \Delta l(0)]\omega}{c} \\ &\approx -\frac{8\pi l_f N\theta(\omega_0 - \omega)}{\omega_0} - \frac{\left(2R\theta^2 - 4x_0\theta\right)\omega}{c}, \end{aligned} \tag{5}$$

where ω is the angular frequency of λ, c is the speed of light in vacuum, and ω_0 is the angular frequency of the pulse's center wavelength λ_0. Eq. (5) confirms that the linear phase ramp is introduced to the laser's spectrum. The group delay g is physically the temporal delay of the pulse envelope which can be found from Eq. (5) to be

$$\begin{aligned} g(t) &= -\frac{\partial p(\omega)}{\partial\omega} \approx \frac{2R{\omega_p}^2}{c}t^2 - \frac{4(l_f N\lambda_0 + x_0)\omega_p}{c}t \\ &= \frac{2R{\omega_p}^2}{c}\left(t - \frac{l_f N\lambda_0 + x_0}{R\omega_p}\right)^2 - \frac{2(l_f N\lambda_0 + x_0)^2}{Rc}, \end{aligned} \tag{6}$$

where ω_p is the angular rotational speed of the polygonal mirror array which is assumed to be constant. The polygonal mirror facet is parallel to the Fourier plane at $t = 0$. Eq. (6) indicates that the temporal delay of the pulse envelope includes a non-negligible quadratic dependence on time [26]. Meanwhile, the duty cycle of the polygonal Fourier-domain delay line can be described in reference to Fig. 2(c). Obviously, all the spectral components imaged onto the Fourier plane should be reflected by the same facet. In the figure, the green and red polygonal shapes represent the start and end of the duty cycle, t_{start} and t_{end}, respectively, which are given by

$$\begin{cases} t_{\text{start}} = -\dfrac{\dfrac{\pi}{P} - \tan^{-1}\left(\dfrac{2x_0 + \Delta h}{2R}\right)}{\omega_p} \approx -\dfrac{\pi}{P\omega_p} + \dfrac{2x_0 + l_f N\Delta\lambda}{2R\omega_p} \\ t_{\text{end}} = \dfrac{\dfrac{\pi}{P} + \tan^{-1}\left(\dfrac{2x_0 - \Delta h}{2R}\right)}{\omega_p} \approx \dfrac{\pi}{P\omega_p} + \dfrac{2x_0 - l_f N\Delta\lambda}{2R\omega_p} \end{cases}, \tag{7}$$

where P is the number of the mirror facets in the polygonal mirror array, $\Delta\lambda$ is the hem-to-hem spectral width of the pulse, and Δh is the geometrical width of the dispersed spectrum in the Fourier plane which can be approximated by $\Delta h \approx l_f N\Delta\lambda$ from the first-order grating equation. The duty cycle D is defined by the effective temporal duration divided by one scanning time $t_{\text{scan}} = 2\pi/P\omega_p$ which is given by

$$D = \frac{t_{\text{end}} - t_{\text{start}}}{t_{\text{scan}}} \approx 1 - \frac{Pl_f N\Delta\lambda}{2\pi R}. \tag{8}$$

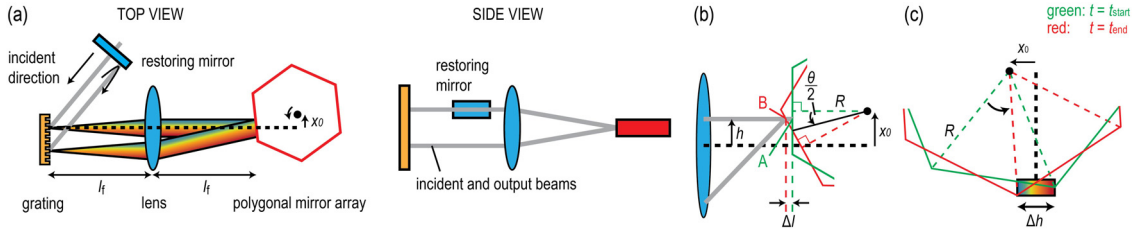

Fig. 2. Polygonal Fourier-domain delay line. (a) Schematic of the polygonal Fourier-domain delay line viewed from the top and side perspectives. To minimize the group-velocity dispersion (GVD) produced by the 4f pulse shaper [26] and enhance the accuracy of Taylor expansions [27], the grating should be placed in parallel to the lens while the center wavelength of the spectrum λ_0 should be normally reflected by the grating to travel through the center of the lens, as shown by the black dashed lines in panels (a), (b) and (c) which reside on the axis of the 4f pulse shaper. (b) Principles of the group-delay generation. (c) Geometrical representation of the duty cycle.

Please cite this article in press as: M. Tamamitsu, et al., Ultrafast broadband Fourier-transform CARS spectroscopy at 50,000 spectra/s enabled by a scanning Fourier-domain delay line, Vib. Spectrosc. (2016), http://dx.doi.org/10.1016/j.vibspec.2016.07.007

2.4. Spectral acquisition parameters

Given Eqs. (1)–(3) and (6)–(8), we discuss the spectral acquisition parameters of the FT-CARS spectroscopy technique such as the spectral resolution and the accessible Raman spectral region. The performance of the system can be maximized by adjusting the position of the reference arm to place the end of the time-domain non-resonant signal (which represents the zero temporal delay between the scanned and reference pulses) at the start of the duty cycle. Eqs. (6) and (7) indicate that the group delays of the start and end of the duty cycle are given by

$$\begin{cases} g(t_{\mathrm{start}}) \approx \dfrac{2R{\omega_{\mathrm{p}}}^2}{\mathrm{c}}\left[\dfrac{-2\pi R - Pl_{\mathrm{f}}N(2\lambda_0 - \Delta\lambda)}{2PR\omega_{\mathrm{p}}}\right]^2 - \dfrac{2(l_{\mathrm{f}}N\lambda_0 + x_0)^2}{Rc} \\ g(t_{\mathrm{end}}) \approx \dfrac{2R{\omega_{\mathrm{p}}}^2}{\mathrm{c}}\left[\dfrac{2\pi R - Pl_{\mathrm{f}}N(2\lambda_0 + \Delta\lambda)}{2PR\omega_{\mathrm{p}}}\right]^2 - \dfrac{2(l_{\mathrm{f}}N\lambda_0 + x_0)^2}{Rc} \end{cases}. \tag{9}$$

The spectral resolution $\delta\nu$ is given by the inverse of the total amount of group delay over the CARS-effective temporal region given by

$$\delta\nu = \left|\frac{1}{g(t_{\mathrm{end}}) - g(t_{\mathrm{start}})}\right| = \left|\frac{cPR}{4l_{\mathrm{f}}N\lambda_0(2\pi R - Pl_{\mathrm{f}}N\Delta\lambda)}\right|. \tag{10}$$

Meanwhile, the down-conversion factor F may be described as a ratio of the total amount of group delay to the effective measurement time given by

$$F = \left|\frac{g(t_{\mathrm{end}}) - g(t_{\mathrm{start}})}{t_{\mathrm{end}} - t_{\mathrm{start}}}\right| = \left|\frac{4l_{\mathrm{f}}N\lambda_0\omega_{\mathrm{p}}}{\mathrm{c}}\right|. \tag{11}$$

Therefore, the higher limit of the accessible Raman spectral region f_{high} is given from Eqs. (2), (3) and (11) by

$$f_{\mathrm{high}} = \min\left(\Delta f_{\mathrm{high}}, \left|\frac{cf_{\mathrm{rep}}}{8l_{\mathrm{f}}N\lambda_0\omega_{\mathrm{p}}}\right|\right). \tag{12}$$

Eqs. (10)–(12) indicate that the performance is insensitive to x_0, which makes our technique easy to use since we do not need to take on a potential technical complexity in measuring or estimating the μm-scale position of the polygonal mirror array while other influential parameters such as the focal length, the groove density, the rotational speed, and the pulse laser's center wavelength and spectral bandwidth are all fixed, readily known values. Qualitatively, this x_0-independence comes from the fact that the relative group-delay evolution follows the same segment of the group-delay curve $g(t)$ regardless of x_0. As shown in Fig. 3(a), Eq. (9) indicates that the relative temporal positions of the start and end of the duty cycle (T_{start} and T_{end}, respectively) with respect to the vertex of the quadratic $g(t)$ curve are fixed against x_0. Meanwhile, the y-coordinate of the vertex (or the offset of the curve) is a function of x_0 which, however, can be neglected as the essence of FT-CARS spectroscopy is the relative evolution of the group delay with respect to the reference pulse. Since the shape of the group-delay curve (which is determined by its quadratic factor of $2R{\omega_{\mathrm{p}}}^2/c$) is also independent of x_0, these features suggest that the relative group-delay evolution follows the same region of the group-delay curve for any value of x_0, and hence the Raman spectral performance of the system remains the same.

2.5. Resampling

We present a resampling procedure that is necessary to retrieve a CARS spectrum with our FT-CARS spectroscopy technique. The nonlinearity of the group delay represented in Eq. (6) means that the molecular vibration is probed with inconstant temporal resolutions, indicating that to retrieve a distortion-free CARS spectrum through Fourier transformation, the CARS interferogram needs to be nonlinearly sampled so that the group-delay differences between any two adjacent sampling points become equal. One way to perform such nonlinear sampling is to digitally resample the time-domain waveform after it is digitized at a constant rate while filling the void between two adjacent digitized points using some approximation such as a polynomial fitting. The procedure is illustrated in Fig. 3(b), based on the curve of $g(t)$ which is sampled with a constant group-delay interval of Δg. Since we have the knowledge that the shape of the group-delay curve is governed by its quadratic factor of $2R{\omega_{\mathrm{p}}}^2/c$, the relative temporal position of the nth resampling point T_{n} with respect to the vertex can be derived as

$${T_{\mathrm{n}}}^2 = {T_{\mathrm{start}}}^2 + \frac{c\Delta g}{2R{\omega_{\mathrm{p}}}^2}n. \tag{13}$$

To use Eq. (13), the only information we need to obtain is the relative position of the start of the duty cycle T_{start} with respect to the vertex. Practically, since it is difficult to directly measure the temporal relation between the reference and scanned pulse trains, a known chemical reagent should be used as an easy calibration reference to determine which of the raw digitized points corresponds to T_{start}, so that the Raman lines are stored at the correct positions on the final CARS spectrum. As T_{start} is determined only by the instrumental parameters, the calibration procedure and its result are solid for all samples.

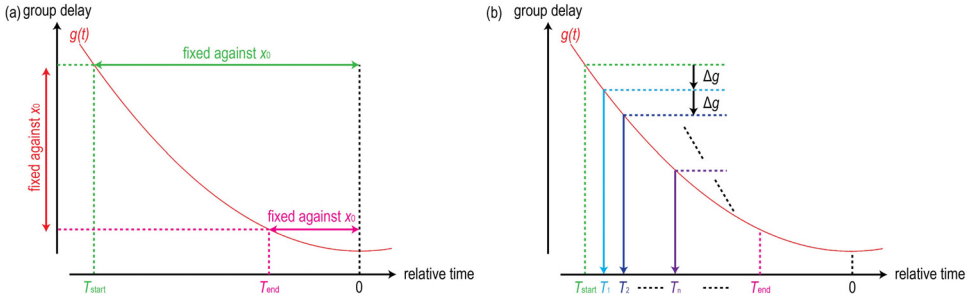

Fig. 3. Analysis of the group delay $g(t)$. (a) Relation between the group-delay curve and the CARS-effective temporal region. The relative positions of the start and end of the duty cycle (T_{start} and T_{end}, respectively) with respect to the vertex of the quadratic group-delay curve are fixed against x_0. This means that the relative group-delay evolution follows the same segment of the group-delay curve regardless of the value of x_0, indicating that the Raman spectral performance is insensitive to x_0. (b) Resampling procedure. The group-delay curve $g(t)$ is resampled with the constant group delay interval of Δg (which is a negative value in the figure) at the start of the duty cycle T_{start}. The relative temporal position of the nth resampling point with respect to the vertex is expressed as T_{n}. Since it is difficult to directly measure the temporal relation between the reference and scanned pulse trains, a known chemical reagent's Raman line should be used as a calibration reference to determine which of the raw digitized points corresponds to T_{start}, so that the Raman lines are stored at the correct positions on the final CARS spectrum.

Please cite this article in press as: M. Tamamitsu, et al., Ultrafast broadband Fourier-transform CARS spectroscopy at 50,000 spectra/s enabled by a scanning Fourier-domain delay line, Vib. Spectrosc. (2016), http://dx.doi.org/10.1016/j.vibspec.2016.07.007

3. Demonstration of FT-CARS spectroscopy with a polygonal Fourier-domain delay line

3.1. Experimental setup

To demonstrate FT-CARS spectroscopy with a polygonal Fourier-domain delay line, we have constructed an optical setup schematically shown in Fig. 4. The femtosecond pulse laser source is Vitara-T-HP (Coherent) which provides an optical spectrum ranging between 740 and 870 nm and f_{rep} = 80 MHz. The laser beam is split into two arms by a polarizing beamsplitter (PBS). A $\lambda/2$ waveplate before the PBS is used to vary the power ratio between the two arms. In the scanning arm, we use a polygonal Fourier-domain delay line consisting of a grating with N = 300 grooves/mm, a lens with a focal length of l_f = 50 mm and a diameter of 30 mm, and a polygonal mirror array [RTA-A54 (Lincoln Laser)] with P = 54 facets, R = 31.8 mm and a rotational speed of 916 rps in the negative scanning direction, corresponding to the scan rate of 50 kHz. Two 50 mm lenses are implemented in the other arm to eliminate the GVD difference between the two arms. A $\lambda/4$ waveplate is placed in both arms to perpendicularly change the polarizations of the beams, so that the returning beams are recombined by the PBS. The combined beams are directed to a pair of dispersion-compensating mirrors which delivers pulses with a temporal duration of ~21 fs in the sample plane. A 750 nm optical long-pass filter is implemented before the sample, permitting the spectral components ranging from 750 nm to 870 nm (corresponding to Δf_{high} = ~1840 cm^{-1}) to induce the CARS process with λ_0 = 810 nm and $\Delta\lambda$ = 120 nm. Two 8 mm aspheric lenses are used to focus the beam to the liquid toluene sample held in a cuvette [21/Q/1 (Starna)] and collect the generated anti-Stokes fields which are extracted by a 750 nm optical short-pass filter. The beam is focused to an avalanche photodiode [APD 120A/M (Thorlabs)] to readout the CARS interferogram which is extracted by an electrical low-frequency-pass filter [DC–48 MHz (Mini-Circuits)]. The detected signal is digitized by ATS9440 (Alzartech) at 125 MHz which is analyzed by a Matlab program on a computer. The incident beam power of ~960 mW results in the scanning beam power of ~120 mW and the reference beam power of ~140 mW at the sample.

3.2. Experimental results

We demonstrate ultrafast broadband Raman spectroscopy with the constructed setup. Fig. 5(a) shows a series of 60 CARS interferograms of the liquid toluene acquired at 50,000 spectra/s. Each of the interferograms is nonlinearly resampled according to Eq. (13) with $\Delta g = 6$ fs, while a linear fitting is used to fill the void between two adjacent points of the digitized raw time-domain waveform. Here the toluene-specific 1003 cm^{-1} Raman line is used as the spectral calibration reference. Fig. 5(b) shows a resampled waveform of one interferogram indicated by the red rectangle in Fig. 5(a). The horizontal axis is replaced by the group delay of the scanned pulse g with respect to the reference pulse on a picosecond scale. The inset shows the enlargement of 0.45 ps $\leq g \leq$ 5.0 p, showing a clear beating pattern characteristic of the toluene which appears after an instantaneous non-resonant peak at $g = 0$ ps. The visible CARS modulation within 0.45 ps $\leq g \leq$ 8.0 ps (indicated by the green arrows) is segmented, triangular-apodized and Fourier-transformed to retrieve the CARS spectrum. Fig. 5(c) shows the obtained CARS spectrum with a spectral resolution of 4.2 cm^{-1} or 7.5 cm^{-1} (apodized). The spectrum has three Raman lines at 786, 1003 and 1030 cm^{-1} which are all characteristic of the toluene. Shown in Fig. 5(d) is an average of 54 continuously acquired spectra. The higher signal-to-noise ratio helps us visualize additional two Raman lines at 521 and 1210 cm^{-1}, showing that the Raman spectral region of at least ≤1210 cm^{-1} is accessible. Finally, Fig. 5(e) shows a series of CARS spectra, each obtained from a different interferogram appearing in Fig. 5(a). One cycle of the color gradient from blue to red includes 54 CARS spectra, corresponding to one complete rotation of the polygonal mirror array. The figure shows that all the 54 polygonal facets reproduce the toluene-specific CARS spectrum with a high temporal resolution of 20 μs, validating the ability of our FT-CARS spectroscopy technique to perform continuous ultrafast broadband Raman spectroscopy.

3.3. Optimization and improvement

For further improvement of the technique, we analyze the obtained data in terms of (1) duty cycle and spectral resolution, (2) accessible Raman spectral region, and (3) spectral distortion. By addressing the issues below, our technique has the potential to cover the entire molecular fingerprint region at least up to 1840 cm^{-1} with a higher spectral resolution of 3.4 cm^{-1} without sacrificing the spectral acquisition rate while also reducing some artifacts appearing in the obtained CARS spectrum. We expect that not only its high-speed spectral acquisition capability, but also these broadband and high-resolution features make our technique more powerful for high-speed chemical analysis.

3.3.1. Duty cycle and spectral resolution

While Eq. (8) indicates that the duty cycle of our setup is calculated to be 51%, the visible CARS modulation in the raw time-domain waveform lasts for ~44% of one scanning time, yielding a non-optimum spectral resolution of 4.2 cm^{-1}. We think this can be

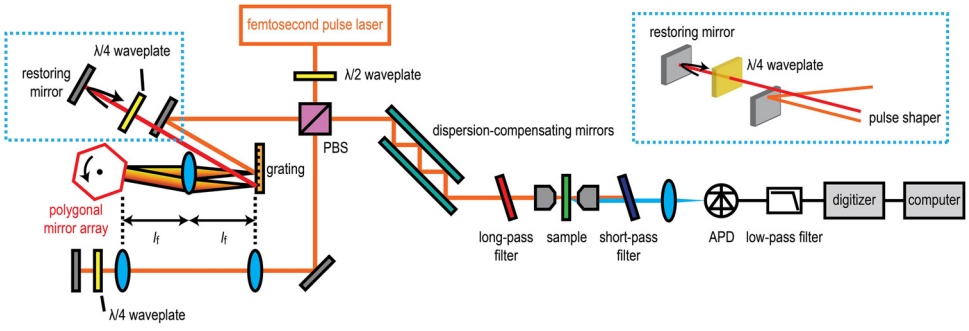

Fig. 4. Schematic of the FT-CARS spectroscopy system with the polygonal Fourier-domain delay line. The blue dotted rectangle is enlarged to show in the inset that the first output beam from the 4f pulse shaper travels at a higher position than the incident beam so that it can be restored by the restoring mirror regardless of the sign of the reflecting angle θ. PBS: polarizing beamsplitter, APD: avalanche photodiode. (For interpretation of the references to colour in this figure legend, the reader is referred to the web version of this article.)

Please cite this article in press as: M. Tamamitsu, et al., Ultrafast broadband Fourier-transform CARS spectroscopy at 50,000 spectra/s enabled by a scanning Fourier-domain delay line, Vib. Spectrosc. (2016), http://dx.doi.org/10.1016/j.vibspec.2016.07.007

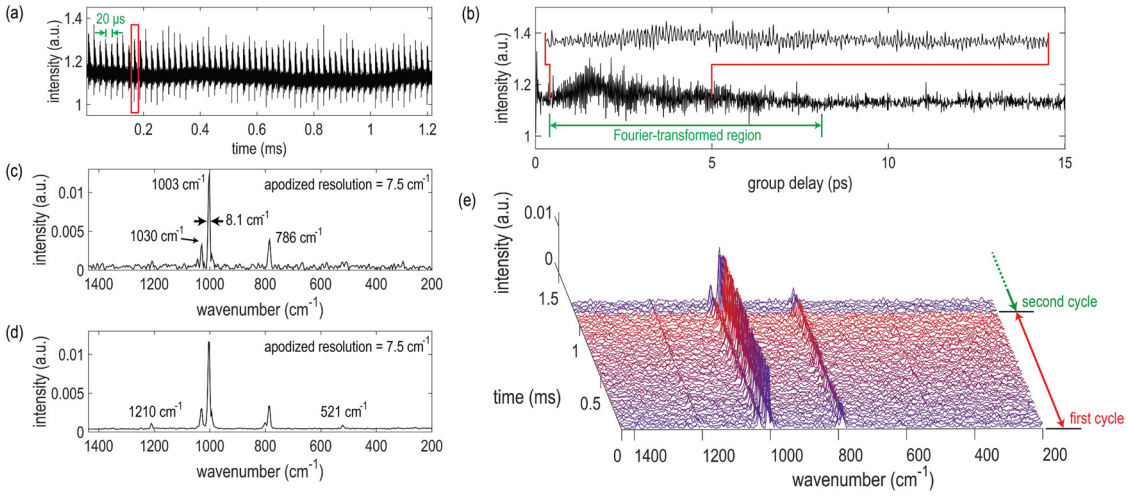

Fig. 5. Ultrafast broadband Raman spectroscopy with our FT-CARS spectroscopy system. (a) Series of 60 toluene CARS interferograms continuously acquired at 50,000 spectra/s. (b) One resampled CARS intereferogram indicated by the red rectangle in Fig. 5(a). The horizontal axis is replaced by the group delay of the scanned pulse with respect to the reference pulse to present the true waveform of the molecular vibration. (c) CARS spectrum of the toluene obtained by Fourier-transforming the visible CARS modulation indicated by the green arrows in Fig. 5(b). Three Raman lines at 786, 1003 and 1030 cm^{-1} are visible. The spectral resolution is 4.2 cm^{-1} or 7.5 cm^{-1} (apodized). (d) Averaged CARS spectrum of the toluene, showing additional two Raman lines at 521 and 1210 cm^{-1}. (e) Series of 60 toluene CARS spectra obtained from the CARS intereferograms shown in Fig. 5(a). One cycle of the color gradient from blue to red includes 54 spectra, showing that all the 54 facets of the polygonal mirror array reproduce the toluene-specific CARS spectrum with the temporal resolution of 20 μs. (For interpretation of the references to colour in this figure legend, the reader is referred to the web version of this article.)

improved by optimizing the 4f pulse shaper; in the current setup, the output beam's path from the pulse shaper laterally shifts as the polygonal mirror array rotates. This results in poorer overlapping between the reference and scanned beams when $|\theta| > 0$, restricting the CARS generation at a large $|t|$. Optimum alignment of the 4f pulse shaper may reduce the lateral shifting to improve the spectral resolution up to 3.4 cm^{-1} as calculated in Eq. (10). Moreover, Eq. (8) indicates that the use of a shorter focal length l_f and/or a lower grating frequency N can further enhance the duty cycle, hence the spectral resolution without sacrificing the spectral acquisition rate.

3.3.2. Accessible Raman spectral region

We also discuss the technique's capability of broadband Raman spectral acquisition. While our experimental demonstration only shows Raman lines residing between 521–1210 cm^{-1}, Eq. (2) indicates that a Raman spectral region of up to 1840 cm^{-1} is accessible with the excitation pulse's bandwidth. However, a low pulse repetition frequency of 80 MHz gives a more strict limitation, making the Raman spectral region above 1430 cm^{-1} inaccessible [Eq. (12)]. The use of a 100 MHz pulse laser with the same optical spectrum enables full utilization of the design parameters, covering the whole molecular fingerprint region without sacrificing the spectral resolution. The use of a shorter optical pulse source such as a few-cycle pulse laser can expand the Raman spectral bandwidth beyond 3000 cm^{-1}; however, it comes at the expense of the duty cycle, hence the spectral resolution, as Eqs. (8) and (10) indicate.

3.3.3. Spectral distortion

Finally, we discuss the origin of the spectral distortion appearing in the obtained CARS spectra. The full-width-at-half-maximum width of the 1003 cm^{-1} line in Fig. 5(c) is 8.1 cm^{-1} which is broader than the apodized spectral resolution of 7.5 cm^{-1}, while a sideband feature is visible on the left or right side of the Raman line at 786 or 1003 cm^{-1} in Fig. 5(d), respectively. This degraded spectral performance is presumably the result of the resampling where we employed a linear approximation between two adjacent points of the digitized raw time-domain signal. Since Eq. (11) indicates that the Raman line of, e.g., 786 cm^{-1} has the down-converted frequency of ~22 MHz, the digitizing frequency of 125 MHz may not be sufficient for the linear approximation. The use of a relatively higher digitizing frequency (e.g., >1 GHz) or a real-time analog phase-correcting sampling technique [25] may improve the accuracy of the resampling and reduce the spectral distortion.

4. Conclusions

In conclusion, we have demonstrated broadband Raman spectroscopy over the expected Raman spectral region of 200–1430 cm^{-1} with the resolution of 4.2 cm^{-1} at an ultrahigh scan rate of 50,000 spectra/s. This record-high Raman spectral acquisition over most of the molecular fingerprint region is enabled by our FT-CARS spectroscopy technique based on the use of a polygonal Fourier-domain delay line. The ultrahigh scan rate is realized by the combination of a fast mechanical rotation and a polygonal geometry of the mirror array. While the nonlinear increase of the group delay produced by the polygonal Fourier-domain delay line requires a nonlinear sampling of the CARS interferogram, we have experimentally shown that an analyzable CARS spectrum can still be retrieved from a constantly digitized waveform by using a theoretically predictable nonlinear resampling approach. While some spectral distortion is expected to occur due to the resampling technique, we assume it can be reduced by digitizing the analog signal at a higher sampling rate or employing a real-time analog phase-correcting sampling technique. Furthermore, optimization of and minor modification to the setup (such as the use of a higher-repetition-frequency pulse laser accompanied by a shorter focal length and/or a lower grating frequency of the 4f pulse shaper) can improve its performance, covering the whole molecular fingerprint region up to 1840 cm^{-1} with the spectral resolution less than 3.4 cm^{-1} without sacrificing the spectral acquisition rate. Such an ultrafast, broadband, high-resolution Raman spectroscopy platform would be of great use in applications where high-throughput screening or real-time monitoring of unknown samples with high specificity is required, such as single-cell analysis and biomedical imaging.

Please cite this article in press as: M. Tamamitsu, et al., Ultrafast broadband Fourier-transform CARS spectroscopy at 50,000 spectra/s enabled by a scanning Fourier-domain delay line, Vib. Spectrosc. (2016), http://dx.doi.org/10.1016/j.vibspec.2016.07.007

Acknowledgements

This work is supported by the ImPACT program (Cabinet Office, Government of Japan). K. Goda is partly supported by Burroughs Wellcome Foundation.

References

[1] T.T. Le, S. Yue, J. Cheng, Shedding new light on lipid biology with coherent anti-Stokes Raman scattering microscopy, J. Lipid Res. 51 (2010) 3091, doi:http://dx.doi.org/10.1194/jlr.R008730.
[2] M.C. Wang, W. Min, C.W. Freudiger, G. Ruvkun, X.S. Xie, RNAi screening for fat regulatory genes with SRS microscopy, Nat. Methods 8 (2011) 135, doi:http://dx.doi.org/10.1038/nmeth.1556.
[3] W. Min, C.W. Freudiger, S. Lu, X.S. Xie, Coherent nonlinear optical imaging: beyond fluorescence microscopy, Annu. Rev. Phys. Chem. 62 (2011) 507, doi:http://dx.doi.org/10.1146/annurev.physchem.012809.103512.
[4] C. Chung, J. Boik, E.O. Potma, Biomolecular imaging with coherent nonlinear vibrational microscopy, Annu. Rev. Phys. Chem. 64 (2013) 77, doi:http://dx.doi.org/10.1146/annurev-physchem-040412-110103.
[5] D. Fu, J. Zhou, W.S. Zhu, P.W. Manley, Y.K. Wang, T. Hood, A. Wylie, W.S. Xie, Imaging the intracellular distribution of tyrosine kinase inhibitors in living cells with quantitative hyperspectral stimulated Raman scattering, Nat. Chem. 6 (2014) 614, doi:http://dx.doi.org/10.1038/NCHEM.1961.
[6] C.H. Camp, Y.J. Lee, J.M. Heddleston, C.M. Hartshorn, A.R.H. Walker, J.N. Rich, J. D. Lathia, M.T. Cicerone, High-speed coherent Raman fingerprint imaging of biological tissues, Nat. Photon. 8 (2014) 627, doi:http://dx.doi.org/10.1038/NPHOTON.2014.145.
[7] C.H. Camp, M.T. Cicerone, Chemically sensitive bioimaging with coherent Raman scattering, Nat. Photon. 9 (2015) 295, doi:http://dx.doi.org/10.1038/NPHOTON.2015.60.
[8] C. Krafft, B. Dietzek, J. Popp, Raman and CARS microspectroscopy of cells and tissues, Analyst 134 (2009) 1046, doi:http://dx.doi.org/10.1039/b822354h.
[9] F. Legare, C.L. Evans, F. Ganikhanov, X.S. Xie, Towards CARS endoscopy, Opt. Express 14 (2006) 4277, doi:http://dx.doi.org/10.1364/OE.14.004427.
[10] B.G. Saar, C.W. Freudiger, J. Reichman, C.M. Stanley, G.R. Holtom, X.S. Xie, Video-rate molecular imaging in vivo with stimulated Raman scattering, Science 330 (2010) 1368, doi:http://dx.doi.org/10.1126/science.1197236.
[11] B.G. Saar, R.S. Johnston, C.W. Freudiger, X.S. Xie, E.J. Seibel, Coherent Raman scanning fiber endoscopy, Opt. Lett. 36 (2011) 2396, doi:http://dx.doi.org/10.1364/OL.36.002396.
[12] M. Ji, D.A. Orringer, C.W. Freudiger, S. Ramkissoon, X. Liu, D. Lau, A.J. Golby, I. Norton, M. Hayashi, N.Y.R. Agar, G.S. Young, C. Spino, S. Santagata, S. Camelo-Piragua, K.L. Ligon, O. Sagher, X.S. Xie, Rapid, label-free detection of brain tumors with stimulated Raman scattering microscopy, Sci. Transl. Med. 5 (2013) 201ra119, doi:http://dx.doi.org/10.1126/scitranslmed.3005954.
[13] R. Arora, G.I. Petrov, V.V. Yakovlev, M.O. Scully, Detecting anthrax in the mail by coherent Raman microspectroscopy, PNAS 109 (2012) 1151, doi:http://dx.doi.org/10.1073/pnas.1115242108.
[14] L. Czerwinski, J. Nixdorf, G.D. Florio, P. Glich, Broadband stimulated Raman microscopy with 0.1 ms pixel acquisition time, Opt. Lett. 41 (2016) 3021, doi:http://dx.doi.org/10.1364/OL.41.003021.
[15] Y. Ozeki, W. Umemura, Y. Otsuka, S. Satoh, H. Hashimoto, K. Sumimura, N. Nishizawa, K. Fukui, K. Itoh, High-speed molecular spectral imaging of tissue with stimulated Raman scattering, Nat. Photon. 6 (2012) 845, doi:http://dx.doi.org/10.1038/NPHOTON.2012.263.
[16] A.M. Weiner, D.E. Leaird, G.P. Wiederrecht, K.A. Nelson, Femtosecond multiple-pulse impulsive stimulated Raman scattering spectroscopy, J. Opt. Soc. Am. B 8 (1991) 1264, doi:http://dx.doi.org/10.1364/JOSAB.8.001264.
[17] A. Volkmer, L.D. Book, X.S. Xie, Time-resolved coherent anti-Stokes Raman scattering microscopy: imaging based on Raman free induction decay, Appl. Phys. Lett. 80 (2002) 1505, doi:http://dx.doi.org/10.1063/1.1456262.
[18] N. Dudovich, D. Oron, Y. Silberberg, Single-pulse coherently controlled nonlinear Raman spectroscopy and microscopy, Nature 418 (2002) 512, doi:http://dx.doi.org/10.1038/nature00933.
[19] J.P. Ogilvie, E. Beaurepaire, A. Alexandrou, M. Joffre, Fourier-transform coherent anti-Stokes Raman scattering microscopy, Opt. Lett. 31 (2006) 480, doi:http://dx.doi.org/10.1364/OL.31.000480.
[20] K. Isobe, A. Suda, M. Tanaka, H. Hashimoto, F. Kannari, H. Kuwano, H. Mizuno, A. Miyawaki, K. Midorikawa, Single-pulse coherent anti-Stokes Raman scattering microscopy employing an octave spanning pulse, Opt. Express 17 (2009) 11259, doi:http://dx.doi.org/10.1364/OE.17.011259.
[21] T. Ideguchi, S. Holzner, B. Bernhardt, G. Guelachvili, N. Picque, T.W. Hansch, Coherent Raman spectro-imaging with laser frequency combs, Nature 502 (2013) 355, doi:http://dx.doi.org/10.1038/nature12607.
[22] S.R. Domingue, D.G. Winters, R.A. Bartels, Time-resolved coherent Raman spectroscopy by high-speed pump-probe delay scanning, Opt. Lett. 39 (2014) 4124, doi:http://dx.doi.org/10.1364/ol.39.004124.
[23] S. Yampolsky, D.A. Fishman, S. Dey, E. hulkko, M. Banik, E.O. Potma, V.A. Apkarian, Seeing a single molecule vibrate through time-resolved coherent anti-Stokes Raman scattering, Nat. Photon. 8 (2014) 650, doi:http://dx.doi.org/10.1038/NPHOTON.2014.143.
[24] C. Liao, P. Wang, P. Wang, J. Li, H.J. Lee, G. Eakins, J. Cheng, Spectrometer-free vibrational imaging by retrieving stimulated Raman signal from highly scattered photons, Sci. Adv. 1 (2015) e1500738, doi:http://dx.doi.org/10.1126/sciadv.1500738.
[25] K. Hashimoto, M. Takahashi, T. Ideguchi, K. Goda, Broadband coherent Raman spectroscopy running at 24,000 spectra per second, Sci. Rep. 6 (2016) 21036, doi:http://dx.doi.org/10.1038/srep21036.
[26] A.L. Oldenburg, J.J. Reynolds, D.L. Marks, S.A. Boppart, Fast-Fourier-domain delay line for *in vivo* optical coherence tomography with a polygonal scanner, Appl. Opt. 42 (2003) 4606, doi:http://dx.doi.org/10.1364/AO.42.004606.
[27] A.V. Zvyagin, E.D.J. Smith, D.D. Sampson, Delay and dispersion characteristics of a frequency-domain optical delay line for scanning interferometry, J. Opt. Soc. Am. A 20 (2003) 333, doi:http://dx.doi.org/10.1364/JOSAA.20.000333.
[28] Y. Yan, E.B. Gamble, K.A. Nelson, Impulsive stimulated scattering: general importance in femtosecond laser pulse interactions with matter, and spectroscopic applications, J. Chem. Phys. 83 (1985) 5391, doi:http://dx.doi.org/10.1063/1.449708.

Please cite this article in press as: M. Tamamitsu, et al., Ultrafast broadband Fourier-transform CARS spectroscopy at 50,000 spectra/s enabled by a scanning Fourier-domain delay line, Vib. Spectrosc. (2016), http://dx.doi.org/10.1016/j.vibspec.2016.07.007